



HAL
open science

Numerical and experimental characterization of twin transmission across grain boundaries along the forward and lateral directions

M. Arul Kumar, K. Dang, Vincent Taupin, R.J. McCabe, C.N. Tomé, L. Capolungo

► To cite this version:

M. Arul Kumar, K. Dang, Vincent Taupin, R.J. McCabe, C.N. Tomé, et al.. Numerical and experimental characterization of twin transmission across grain boundaries along the forward and lateral directions. *Materialia*, inPress, 23, pp.101437. 10.1016/j.mtla.2022.101437 . hal-03807915

HAL Id: hal-03807915

<https://hal.univ-lorraine.fr/hal-03807915>

Submitted on 10 Oct 2022

HAL is a multi-disciplinary open access archive for the deposit and dissemination of scientific research documents, whether they are published or not. The documents may come from teaching and research institutions in France or abroad, or from public or private research centers.

L'archive ouverte pluridisciplinaire **HAL**, est destinée au dépôt et à la diffusion de documents scientifiques de niveau recherche, publiés ou non, émanant des établissements d'enseignement et de recherche français ou étrangers, des laboratoires publics ou privés.



Distributed under a Creative Commons Attribution - NonCommercial - NoDerivatives 4.0 International License

Numerical and experimental characterization of twin transmission across grain boundaries along the forward and lateral directions

M. Arul Kumar^{a,*}, K. Dang^a, V. Taupin^b, R.J. McCabe^a, C.N. Tomé^a, L. Capolungo^a

^a *Materials Science and Technology Division, Los Alamos National Laboratory, Los Alamos, NM 87545, USA*

^b *Arts et Métiers ParisTech, Université de Lorraine, CNRS, LEM3, Metz F-57000, France*

A B S T R A C T

Pervasive deformation twinning and transmission events across grain boundaries (GBs) affect the strength and failure of hexagonal close-packed (HCP) magnesium. A three-dimensional twin can transmit along the twinning shear direction, η_1 (forward), and along the direction perpendicular to both the twinning plane normal and the shear direction, λ (lateral). For the first time, phase-field calculations and electron backscatter diffraction (EBSD)-based statistical analysis are combined to investigate the effect of the twinned grain boundary characteristics on twin transmission (TT) along the forward and lateral directions. This combined analysis reveals that TT propensity decreases with increasing misorientation angle across the GB for both forward and lateral directions. Also, the TT is more favorable along the lateral than along the forward direction. Twin transmission seems harder across GBs with a misorientation axis closer to the twin λ -direction than the other directions (κ_1 and η_1). Further, the PF calculations reveal that, at the onset of a transmission process, the crystallography tends to be preserved in the case of lateral transmission, whereas, in the forward transmission case, the transmitted twin punches straight through the GBs and its morphology prevails. The EBSD analysis finds that pure forward and lateral transmissions do not occur often, yet reveals a preference for lateral propagation consistent with PF simulations. Further, the local twin transmission configurations observed in the actual material do not correspond to pure tilt or twist GBs, which are most commonly considered as model cases.

1. Introduction

Hexagonal close-packed (HCP) magnesium and its alloys activate deformation twinning in addition to dislocation slip when strained. Deformation twins nucleate as embryos at grain boundaries (GB) where suitable defect structures and stress concentrations are primarily located [1–5]. Under further straining, twins propagate into grains and terminate at opposing GBs. Due to their three-dimensional nature, deformation twins propagate in directions perpendicular to the twinning plane normal, κ_1 , including along the twinning shear direction (η_1) and the λ ($= \kappa_1 \times \eta_1$) direction, which is perpendicular to κ_1 and η_1 [6,7]. In this work, twin propagation along the η_1 and λ directions are referred to as forward and lateral propagation, respectively. Following propagation, a twin grows in thickness in the κ_1 normal direction [8–10]. Often, twins propagate further across GBs. These events are referred to as twin transmission (TT). The TT process may continue over several grains developing long twin chains. TT increases the likelihood of instabilities like crack propagation and premature failure [11–13].

In principle, TT can occur in any direction contained in the twinning plane, and it is expected that most TT events will not be exactly in the

forward or lateral directions. Recent studies [14–17] suggest that, based on mobility and local twinning-induced internal stresses, (1) twin propagation is easier along the lateral direction than along the forward direction, and (2) the propagation rate along any other direction is bounded by the forward and lateral directions. Thus, it is likely that TT propensity is bounded by limit cases corresponding to forward and lateral interactions of a twin domain with a grain boundary. These bounding cases are investigated here using phase-field simulations. Precisely, TT along the shear direction η_1 (forward twin transmission, FTT) and along the λ direction (lateral twin transmission, LTT) is simulated for various GB configurations.

Naturally, it is necessary to comprehensively quantify, from a statistical standpoint, the geometry of TT events and the probability of successful FTT and LTT in actual material systems. This is key to determining whether preferential pathways for twin transmission exist as a function of the relative GB/twin geometry. To capture GB/Twin geometry effects, twins need to be characterized in 3D, which is challenging with current experimental tools. Only a few studies have attempted to reveal experimentally the 3D morphology of twins in HCP polycrystals [18,19]. These studies were able to reconstruct only a few twins, which is insufficient to derive any reliable statistical correlations. Instead, 2D

analysis of two or three specific orthogonal sections of a 3D volume can help in understanding the 3D characteristics of twins and their transmission [6,7]. For example, Liu et al. [7] statistically analyzed 3D twin morphologies and sizes using three different sample slices, while Wang et al. [20,21] have characterized the twin facets of 3D tensile and compressive twins in Mg and Ti, respectively. In this work, two different sections of a 3D microstructure are considered to explore the transmission of tensile twins in Mg in the forward and lateral directions.

TT processes are known to be strongly correlated with GB characteristics such as misorientation angle and axis. Studies of TT across GBs have predominantly considered only FTT or have disregarded the TT direction. TT has been studied in a variety of HCP metals, including magnesium and its alloys [22–30], zirconium [27], titanium and its alloys [31,32], and rhenium [33]. The most common feature from all of these studies is that the TT frequency decreases with increasing misorientation angle across GBs. To the best of our knowledge, the present study is the first characterizing TT in both forward, η_1 , and lateral, λ , directions.

To address the points mentioned above, a combined phase-field modeling and Electron Back Scatter Diffraction (EBSD)-based statistical analysis of twins is performed. In the phase-field model, the transmission of twins across GBs in the forward and lateral directions is explicitly simulated for a series of GB characteristics (misorientation angles and axes). Note that the considered GBs are symmetric tilt and twist boundaries about special crystallographic axes. For the EBSD-based statistical analysis, strongly basal-textured commercial purity magnesium is compressed along the rolling direction (RD) to 1% strain to activate $\{10\bar{1}2\}$ tensile twins. EBSD images are obtained from two different sections of the polycrystal and analyzed using an automated twinning analysis software, METIS [34], to capture TT along directions close to the forward and the lateral ones. This combined study addresses the following key questions: (i) is TT more favorable along the forward or lateral direction? (ii) what is the relationship between GB characteristics (misorientation angle and axis) and the likelihood of FTT and LTT? Further, EBSD-based statistical analysis helps to answer the following questions: (iii) how often the considered special symmetric GBs are observed in the actual material? (iv) what is the probability of FTT and LTT events in the actual deformed microstructure?

The paper is structured as follows. In Section 2, the phase-field model is briefly described. Section 3 presents the initial material, microstructure imaging, and statistical analysis. The phase-field model results and the key findings are presented in Sections 4.1 and 4.2. EBSD-based statistical analysis of TT events is presented in Section 4.3. Finally, conclusions are summarized in Section 5.

2. Phase-field modeling

A recently developed phase-field framework that simulates the 3D growth of an isolated twin domain is employed here [14,16,17]. In this model, the interfacial energies and mobilities of the facets that bound the twin domain are explicitly considered. Critically, the model was shown to be able to replicate the twin growth kinetics and anisotropy in excellent agreement with atomistic simulations [16,17]. For the sake of completeness, it is briefly summarized below.

The non-conservative (i.e., Allen Cahn type) phase-field model is set on a regular Fourier grid with a spatial resolution of 0.401 nm to avoid numerical pinning. For every voxel, a phase variable, ϕ , which quantifies the twin volume fraction in that voxel, is considered. A value of $\phi = 0$ indicates the voxel is purely matrix, and a value of $\phi = 1$ indicates the voxel is purely twin. Any value in between indicates the voxel is part of the twin interface. To evolve the phase variable, the Helmholtz free energy F is calculated. The latter consists of the following three components: the elastic strain energy E , the interfacial barrier energy f , and the interfacial gradient energy Γ . Together, the free energy is given by

$$F = \int \int \int_V (E + f + \Gamma) dV \quad (1)$$

Table 1

Possible $\{10\bar{1}2\}$ tensile twin domain facets and their interfacial energies [17].

Facet	Index	Energy (J/m^2)
CTB	$\{\bar{1}012\} \parallel \{\bar{1}0\bar{1}2\}$	0.149
BP	$\{0002\} \parallel \{\bar{1}0\bar{1}0\}$	0.122
FTB	$\{\bar{1}012\} \parallel \{\bar{1}012\}$	0.149
A	$\{\bar{1}456\} \parallel \{\bar{1}456\}$	0.123
B	$\{\bar{1}121\} \parallel \{\bar{1}103\}$	0.130
Tilt-PyPy1	$\{\bar{0}111\} \parallel \{\bar{0}111\}$	0.112
C	$\{\bar{0}110\} \parallel \{\bar{1}212\}$	0.105
D	$\{\bar{1}432\} \parallel \{\bar{1}432\}$	0.092
Twist-PyPy1	$\{\bar{1}101\} \parallel \{\bar{0}111\}$	0.112
Twist-PrPr2	$\{\bar{1}210\} \parallel \{\bar{1}210\}$	0.096

The elastic strain energy ($E = \frac{1}{2}\epsilon^e : C : \epsilon^e$) is a contraction of the local elastic strain, ϵ_e , and the local stiffness tensor C . The stiffness tensor is an interpolation of the twin and matrix tensors, respectively, based on the fractional value of ϕ at the voxel in question. Accordingly, the elastic strain and stiffness tensors are written as

$$\epsilon^e = \epsilon - h(\phi)\epsilon^{tw} \text{ and } C = (1 - h(\phi))C^M + h(\phi)C^{tw} \quad (2)$$

The interpolation function $h(\phi)$ and its derivative $h'(\phi)$ are given by,

$$\begin{aligned} h(\phi) &= \phi^2(3 - 2\phi) \\ h'(\phi) &= \frac{\partial h}{\partial \phi} = 6(\phi - \phi^2) \end{aligned} \quad (3)$$

The interfacial barrier and gradient energies, respectively, are given by

$$f(\phi) = W\phi^2(1 - \phi)^2 \quad (4)$$

$$\Gamma = \frac{1}{2}\kappa|\nabla\phi|^2 \quad (5)$$

In Eq. (4), the term W is an energy barrier height for a double-well potential with a value of $7.5 \cdot 10^8 J/m^3$. In Eq. (5), the coefficient κ includes dependence on $\nabla\phi$ to introduce an orientation-dependent interfacial energy $\gamma(\nabla\phi)$ through [17]

$$\kappa = \frac{18\gamma^2}{W} \quad (6)$$

The interfacial energy for all possible $\{10\bar{1}2\}$ twin domain facets are listed in Table 1. The phase variable is evolved following the Allen-Cahn equation [35]

$$\frac{d\phi}{dt} = -L \frac{\partial F}{\partial \phi} \quad (7)$$

Where L is the facet mobility, which also includes a dependence on $\nabla\phi$ to introduce anisotropy of facet mobilities. The mobility can be made dependent on the average resolved shear stress along the direction perpendicular to the facets and calibrated from molecular dynamics measurements of facet velocities for different applied stresses and temperatures [17]. The mobility is given as

$$L = \frac{\sqrt{W}v}{6\sqrt{2}\sqrt{\kappa\sigma\epsilon}} \quad (8)$$

where v is the velocity of a facet for an applied shear stress σ (both values can be obtained from molecular dynamics [39]) and $\epsilon = 0.065$ is the magnitude of the twinning plastic shear strain. Note that the short-range interaction between the GB and twin tip is not considered here and thus the energy of the facets that bound the twin tip is the same before and after the interaction. Thus, one can only assess the effects of geometry and internal stress on twin transmission using this phase-field calculations.

3. Experiment

A commercially pure, fully recrystallized rolled magnesium plate with a strong basal texture is used in this study. The c-axis of the grains are within approximately 30° of the plate normal direction. The initial undeformed microstructure consists of twin-free, equiaxed grains with an average grain size of $70\ \mu\text{m}$. Compression samples with dimensions of $8\ \text{mm}$ (ND) \times $9\ \text{mm}$ (TD) \times $10\ \text{mm}$ (RD) were cut from the rolled plate and compressed in RD to a total strain of 1% to activate $\{10\bar{1}2\}$ tensile twins. Here, ND, TD, and RD denote the normal, transverse, and rolling directions of the magnesium plate. As mentioned in Section 1, two different slices were considered to capture twin transmission events in the forward and lateral directions. Accordingly, one cube was cut in half perpendicularly to the TD such that the sampling plane contains both the ND and RD (compression direction), and it is referred to as Section 1. Because of the strong basal texture and RD compression tends to align the c-axis of twins along the RD, it is expected that a large fraction of twins in this section will be viewed close to the lateral direction (λ) of the $\{10\bar{1}2\}$ tensile twins. Thus, we expect to capture more forward transmissions in the η_1 direction, i.e., FTT events. The second cube was cut at approximately 35° to the ND with the sectioning plane containing the TD, and this section is referred to as view-2. Due to the relative orientation of the loading direction orientation with respect to the initial strong basal texture, many twins in this section are viewed along a direction that is close to the twinning shear direction (η_1) of the twins, and thus allows the viewing of lateral twin transmissions in the λ direction. The samples were prepared for EBSD by mechanically grinding and polishing to $1\ \mu\text{m}$ diamond in propylene glycol and then chemically polishing in 10% nitric acid and water for 10 s. The EBSD data was collected in an FEI XL30 FEG-SEM at 20 kV using a $1\ \mu\text{m}$ step size. The EBSD data was post-treated using the OIM Analysis software using a Neighbor CI Standardization with grain tolerance angle of 5° and minimum grain size of 1 pixel. This post-treatment is followed by a Neighbor CI Correlation clean-up with a minimum CI of 0.3. Together, these steps typically alter less than 1% of the data, and any scan where more than 10% of the data is altered is discarded.

4. Results and discussion

4.1. Phase-field modeling of twin transmission

Following Section 2, phase-field calculations are performed to understand TT in the forward and lateral directions and capture its dependence on GB misorientation. To simulate the FTT and LTT events, the model setup is designed so that the normal to the GB interacting with the twin is parallel to either the twinning shear (η_1) or the lateral direction (λ). Note that the potential emission of dislocations from the grain boundary is not taken into account such that the stress state at the tip of the twin will be grossly over-estimated. However, our previous PF based studies [17] reveal that the model calculated stress fields are qualitatively similar to the experimental measurements [9,36–38] and also to model calculations where the plastic dissipation due to dislocation glide is accounted for [8,10,27,39]. Thus, we expect that the current PF model predicted twin transmission propensity results may not change if one considers the slip induced plastic dissipation at the twin tip. Further, as the local interaction between the twin tip and the grain boundary is unknown, the energy landscape is not modified at the grain boundary (i.e., the model does not account for the likely change in grain boundary energy as a twin facet is absorbed; this approximation amounts to assuming null binding energy of a twin tip with a grain boundary).

The orientation of the parent grain is chosen as $(\frac{\pi}{2}, \text{atan}(\frac{c}{a}), \frac{\pi}{2})$ in the Bunge convention, and the simulated twin variant is $(10\bar{1}2)[\bar{1}011]$. $c = 0.521\ \text{nm}$ and $a = 0.321\ \text{nm}$ are the lattice parameters of HCP Mg. This particular combination of parent grain and the twin variant orientations aligns the twin plane normal with the vertical direction. A set

of neighboring grain orientations are selected to capture the relationship between TT and grain misorientation across the GB and will be discussed later. The size of the unit cell is $51.36 \times 51.36 \times 25.68\ \text{nm}$, and it is discretized into $128 \times 128 \times 64$ voxels with the shortest dimension along the twinning plane normal direction. Initially, a $(10\bar{1}2)[\bar{1}011]$ tensile twin is placed at the center of the parent grain with a size of $9.63 \times 9.63 \times 6.42\ \text{nm}$ in the η_1 - λ - κ_1 directions.

To demonstrate the transmission process, the phase-field simulations are first performed for a 25° misorientation with the GB boundary normal parallel to either the λ - or η_1 -directions of the primary twin. The model setup is shown in the first column of Fig. 1. According to twin crystallography, the grains' misorientation axes along the λ - and η_1 -directions correspond, respectively, to tilt and twist type GBs for the forward interaction, and twist and tilt-type GBs for the lateral interaction. Phase-field calculations are performed at 300 K with an imposed simple-shear stress (varying from 850 MPa to 2 GPa) acting on the twin plane in the η_1 -direction. This particular stress value is chosen to keep the simulated twin from detwinning under its internal stresses. Note that the resolved shear stress necessary to stabilize the twin is $\sim 825\ \text{MPa}$, and that this value may vary slightly with the grain boundary misorientation characteristics due to small but non-null image forces.

4.2. Forward versus lateral transmission

Under a constant 1 GPa imposed load, the initially placed twin domain propagates along both forward and lateral directions and eventually makes contact with the GB. The propagation is faster along the lateral direction compared to the forward direction. For example, the time taken to reach the GB in the forward direction for the 25° /tilt and 25° /twist misorientation cases is 184 ns and 180 ns, respectively, see Fig. 1(b) and (f). By comparison, in the lateral direction, it takes only 72 ns and 68 ns for the same GB cases (see Fig. 1(j) and (n)). As discussed in [16,17], the observed differences in the twin propagation rate are associated with the inherent twinning shear-transformation-induced local stress field at the twin tip and the anisotropy in the mobility of the facets in the lateral and forward direction. The twinning-plane resolved shear stress at the twin tip in the forward and lateral directions, which drives the propagation of an isolated twin inside a single crystal, is ~ 0.3 and $1.17\ \text{GPa}$, respectively [17]. Thus, for the same imposed loading, twin propagation is more favorable in the lateral direction than in the forward direction.

Upon further loading, the twin transmits across the GB. After contact with GB, the delay for the FTT across 25° /tilt and 25° /twist boundaries is 12 and 8 ns, respectively. On the other hand, the delay for the LTT is only 4 ns and 8 ns for the same GB cases (see the third column of Fig. 1). This delay could be due to the difference in the driving force for TT across the GB. The TRSS field within and around the twin domain is shown in Fig. 2 for all four cases. Here the TRSS is calculated by subtracting the imposed uniform shear (τ_{imposed}) of 1 GPa from the model calculated twin-plane resolved shear stress ($\tau_{\eta_1-\kappa_1}$). This gives the intrinsic twinning shear-induced local stress without having a contribution from the imposed load. The stress fields shown in Fig. 2 correspond to the stage of the twin that just touches the GB (second column of Fig. 1). Slice-1 in Fig. 2 is taken at the center of the 3D unit cell so that the primary twin propagation direction (η_1 or λ) is within this slice. In contrast, slice-2 is taken at a voxel just right to the GB in the neighboring grain. This slice provides the available/effective driving force for TT. Fig. 2 clearly shows that the available driving stress for TT is much higher in the lateral direction compared to the forward direction. Thus, TT starts earlier in the lateral direction than in the forward direction. With continued loading, the transmitted twin propagates into the grain and adopts a complex 3D morphology, which is shown in the last column of Fig. 1. It clearly shows the effect of twist versus tilt misorientation axis and transmission direction on twin morphology, which requires detailed characterization.

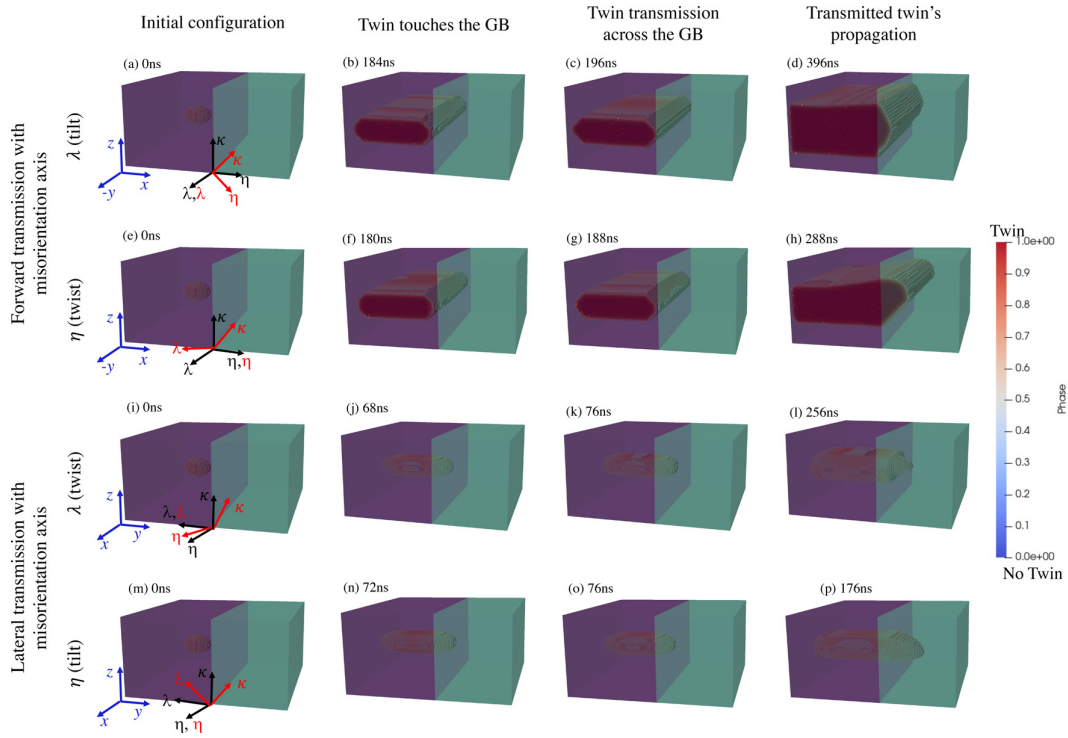


Fig. 1. Phase-field model calculations of twin transmission in the forward (top two rows) and lateral (bottom two rows) directions across 25° misorientation angle GB with two different misorientation axes: λ - and η_1 -directions of the simulated twin. Crystal orientations of the parent (in black) and neighboring grain (in red) are represented using the twin frame. The first, second, third, and fourth columns correspond to the initial configuration, when the twin touches the GB, the twin starts transmitting across the GB, and the transmitted twin propagates into the grain, respectively. Corresponding times for all of these stages are indicated in the frames.

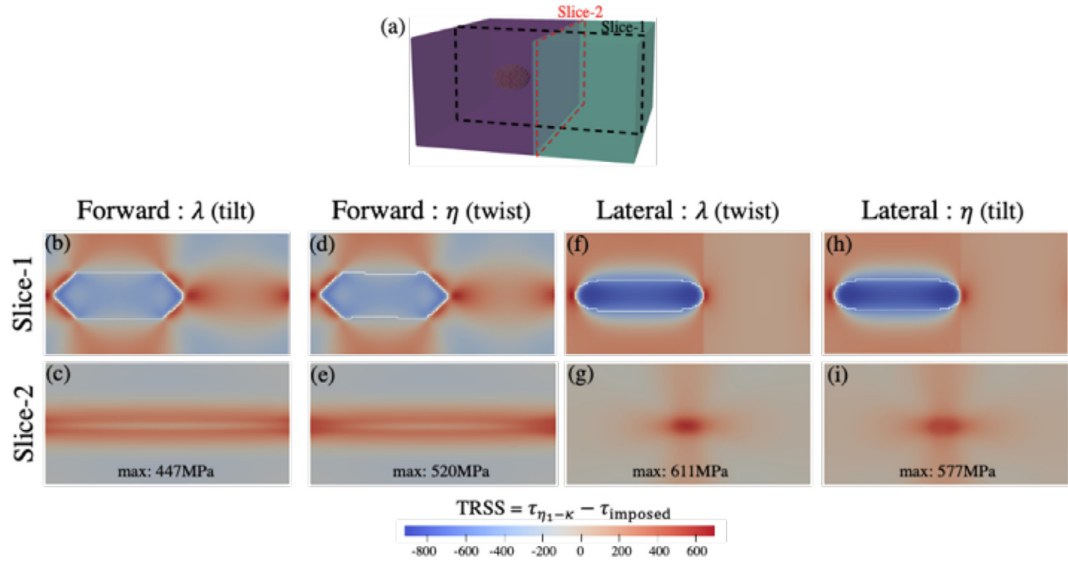


Fig. 2. Phase-field model predicted TRSS field (in MPa) when twin touches the GB. (a) The schematic depicts the location where the slices were taken. The top and bottom row shows the TRSS field from slice-1 and slice-2, respectively. Here the TRSS is calculated by subtracting the imposed shear, τ_{imposed} , from the model calculated twin-plane resolved shear stress, $\tau_{\eta_1-\kappa_1}$.

4.3. Transmitted twin morphology

To understand the morphology of the transmitted twin, 2D sections of the 3D simulation cell are plotted in Fig. 3. Similar to Fig. 1, the four columns of Fig. 3 correspond to different simulation stages: initial

configuration, when the twin touches and crosses the GB, and further propagation into the neighboring grain. Again, the top and bottom two blocks correspond to FTT and LTT, respectively. The first row of the top and bottom two blocks show the twin morphology when viewed along the λ and η_1 directions, respectively. The second rows of each block

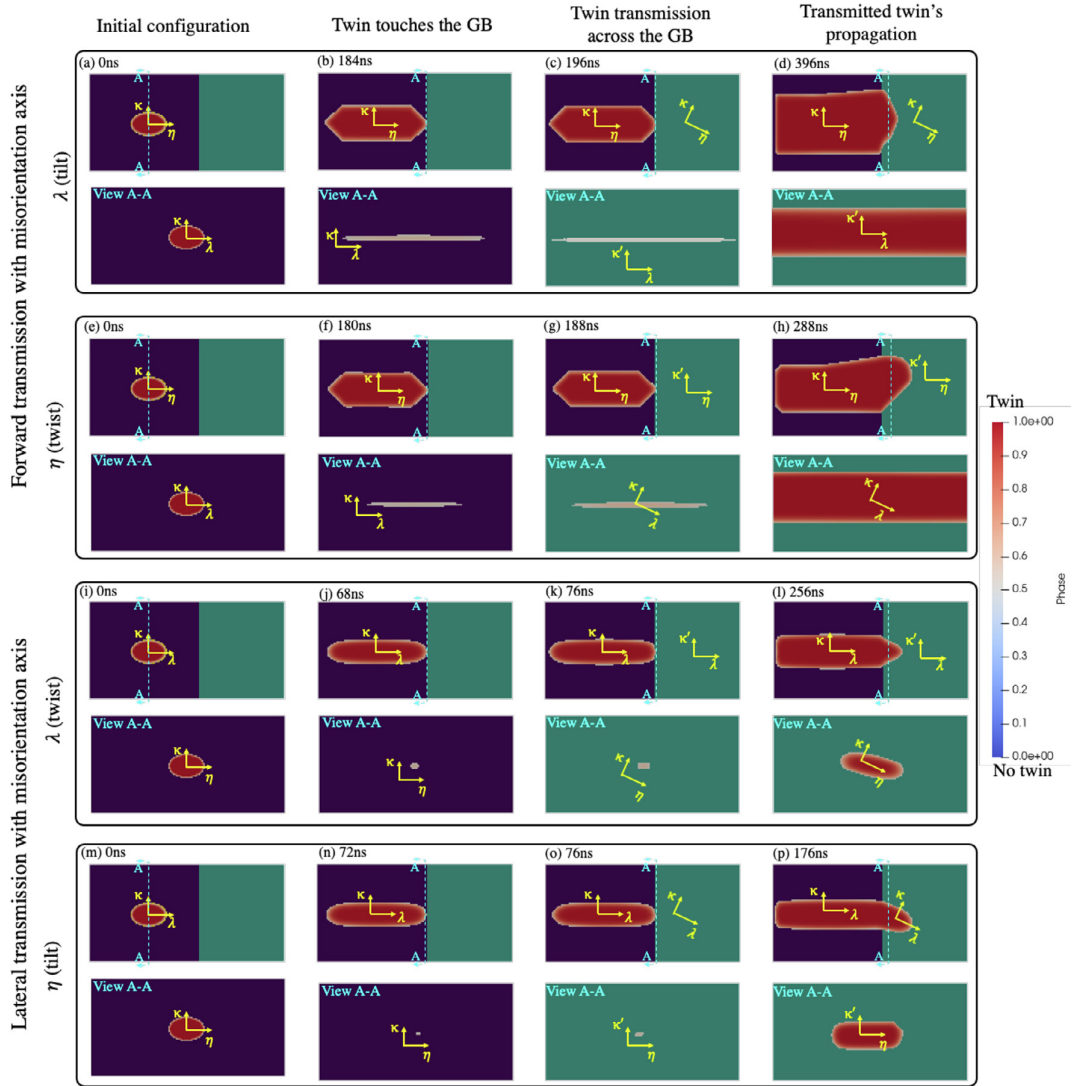


Fig. 3. Phase-field calculations predicted twin morphology at different stages of the FTT and LTT simulations for two different misorientation cases. The cases considered here is the same as the one shown in Fig. 1.

show the twin morphology in slice A-A, which is marked in Fig. 3. Slice A-A is taken at different positions for different stages of the simulation. In the first column, slice A-A is taken at the center of the left side grain to show the initial twin morphology in the forward or lateral directions. In the second column, the slice A-A is taken at a voxel just to the left of the GB to show how the twin makes contact with the GBs. Slice A-A in the third column is taken at a voxel just to the right of the GB to show how the twin is transmitting into the neighboring grain. Slice A-A in the last column is taken at a distance of 1.065 nm from the GB (i.e., fifth voxels from the GB) to see the transmitted twin morphology inside the neighboring grain.

As mentioned before, the starting ellipsoidal twin is slightly shorter in the κ_1 direction. For both misorientation cases, a long CTB is formed before the twin touches the GB in the forward direction, but not so in the lateral direction. This can be explained by the differences in the propagation rate in the forward and lateral directions. For fixed stress and temperature, the time required by a twin to reach the GB in the forward direction is almost three times that in the lateral direction, which gives sufficient time to propagate along the slower κ_1 direction. Interestingly, when the twin touches the GB, the contact region is significantly

larger for the forward interaction than the lateral one for tilt and twist misorientation cases (see the second column of Fig. 3). This is due to the fact that the twin propagates more easily along the lateral direction than the forward direction. Further, the long dimension of the contact region for the forward and lateral direction cases aligns with the λ and η_1 directions, respectively.

Now, the morphology of the transmitted twin is discussed. Similar to the primary twin, the propagation of the transmitted twin into the neighboring grain in the forward direction is relatively slow compared to the lateral direction. The propagation of the transmitted twin is confined to its crystallographic directions for the LTT, but not for the FTT, something which can be readily seen from the third and fourth columns of Fig. 3. Precisely, in the case of FTT, the transmitted twin propagation direction is not aligned with its η_1 direction and the long dimension of the twin is not aligned with its λ or η_1 directions. Rather, the morphology of this twin looks like an extension of the initial twin-GB contact region, i.e., the twin just punches straight into the neighboring grain. On the other hand, in the case of LTT, the transmitted twin propagation direction for both misorientation cases aligns with the λ direction. Also, the long dimensions of the twin align with its λ and η_1 directions. Further,

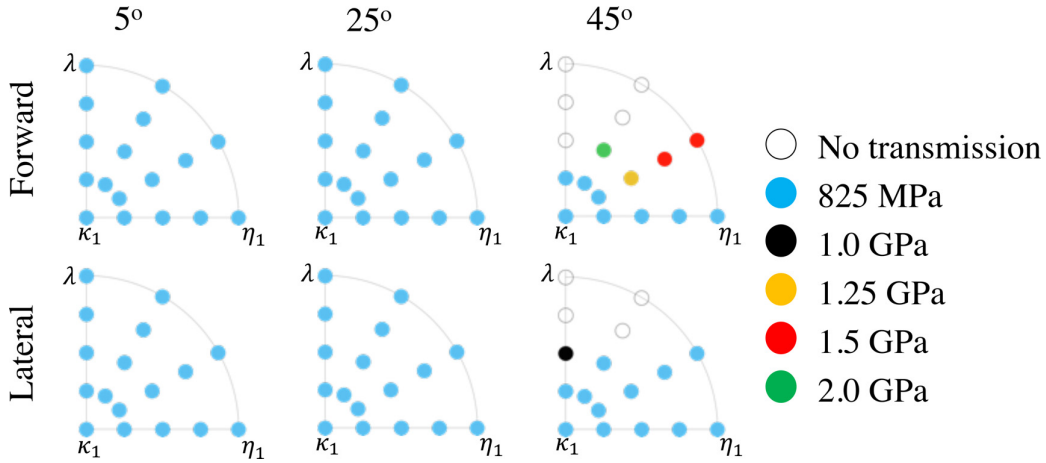


Fig. 4. Phase-field model predicted twin transmissibility in the forward and lateral directions at 300 K for different misorientation axes and angles. For every misorientation angle, each solid point on the pole figure represents a misorientation axis of a GB for which the twin transmission occurs. Whereas the empty points correspond to the cases where twins do not transmit across the GB. The color scheme for the filled points shows the minimum stress required for twin transmission to occur. The top row shows the forward transmission, while the bottom row shows the lateral transmission.

note that the morphology of the primary twin is changed upon transmission in the case of FTT, not in the case of LTT. From these results, one could postulate that, prior to adopting a morphology conforming to the crystallography of the transmitted twin domain, the transmitted twin propagation/growth follows its crystallography in the case of LTT, whereas, for the FTT case, the transmitted twin could punch straight through the GB, and its morphology follows the initial twin and GB contact region.

4.4. Effect of GB characteristics (misorientation angle and axis)

To compare the twin transmissibility in the forward and lateral directions, we have repeated the calculations for different combinations of misorientation angles and axes. To accomplish this, a total of 102 configurations were considered across a wider range of misorientation axes and angles for both forward and lateral directions. Specifically, 17 different misorientation axes were selected to cover the misorientation space for each misorientation angle of 5°, 25° and 45°. Here, misorientation angles only up to 45° were considered. Only where twin transmission co-exists with the slip transmissions. The reason is that our previous atomistic calculations [16] reveal that for misorientation angles below 45° twin transmission co-exists with slip transmissions, while above 45° twin-GB interaction is accommodated mostly by the nucleation and emission of slip dislocations in the neighboring grain, rather than twin transmission. Since, the plasticity due to the slip dislocations is not considered in the model, twin transmission simulations are performed only up to 45° misorientation. To quantify the minimum stress required for twin transmission to occur, PF simulations were performed for the following imposed stresses (MPa): 825, 855, 900, 950, 1000, 1250, 1500, 1750 and 2000.

The simulated configurations and predicted twin transmissibility for both forward and lateral directions are plotted in the $\eta_1 - \lambda - \kappa_1$ space of the twin for different misorientation angles in Fig. 4. Each point in Fig. 4 corresponds to a considered misorientation axis. The selected 17 misorientation axes cover the misorientation space and include the special cases of misorientation about η_1 , λ , or κ_1 . The misorientation about η_1 gives twist and tilt GBs for the forward and lateral transmissions, respectively. The misorientation about λ corresponds to tilt and twist GBs for the forward and lateral transmissions, respectively. The empty and filled circles correspond to scenarios where the twin touches the GB but does not transmit and where the twin transmits, respectively. The color scheme for the filled symbols provides the minimum stress required for

twin transmission to occur. These predictions reveal the following: (i) for both forward and lateral directions, the stress required for twin transmission increases with misorientation angle. In other words, twin transmission propensity decreases with increasing misorientation angle. (ii) TT is favorable in the lateral direction compared to the forward direction; (iii) both FTT and LTT are less likely for misorientation axes closer to the λ -direction.

4.5. EBSD based statistical analysis

The simulation results presented in the previous sections provide the propensity of TT for the bounding cases of forward and lateral transmission as a function of the misorientation angle and axis between the neighboring grains. In this section, using EBSD-based statistical analysis of the deformed microstructure, the probability of developing these bounding TT events and their dependency on GB characteristics are analyzed. As mentioned in Section 3, two different sections are considered for EBSD imaging to capture TT events in different directions. Fig. 5 shows representative EBSD images from both sections. TT events are observed in both sections, and a few TTs are marked by black arrows. To correlate TT events with microstructural features, a large number of grains and twins need to be analyzed. Thus, a total of twelve and eleven distinct scans were acquired, giving combined scan areas of 8.99 and 11.62 mm² for sections-1 and 2, respectively. The collected EBSD scans were analyzed using the automated EBSD-based twinning software METIS to develop statistical correlations [34]. By combining EBSD images from both sections, we have analyzed a total of 3437 grains and 7222 twins. In the analysis, grains with areas less than 4 μm^2 are disregarded. The 7213 $\{10\bar{1}2\}$ tensile twins occupy an area fraction of 7.42% of the total EBSD microstructure. From the postmortem analysis of deformed microstructures, it is challenging to distinguish TT across the GBs from simultaneously (co-) nucleated twins at a common GB emitted into both grains. For the sake of simplicity, twins connected at a common GB are associated with a TT event in this work. From the statistical analysis, a total of 1708 adjoining twin pairs (ATPs) was observed in the collected EBSD images.

Before analyzing the TT process in the forward and lateral directions, twin-GB interactions are classified based on the direction in which they interact with the GBs. In this work, a twin is classified as forward twin (FT) if its twinning shear direction, η_1 , is interacting with the GB, whereas twin is classified as lateral twin (LT) if its lateral direction, λ , is interacting with the GB. In other words, a twin is labeled as a FT if it's

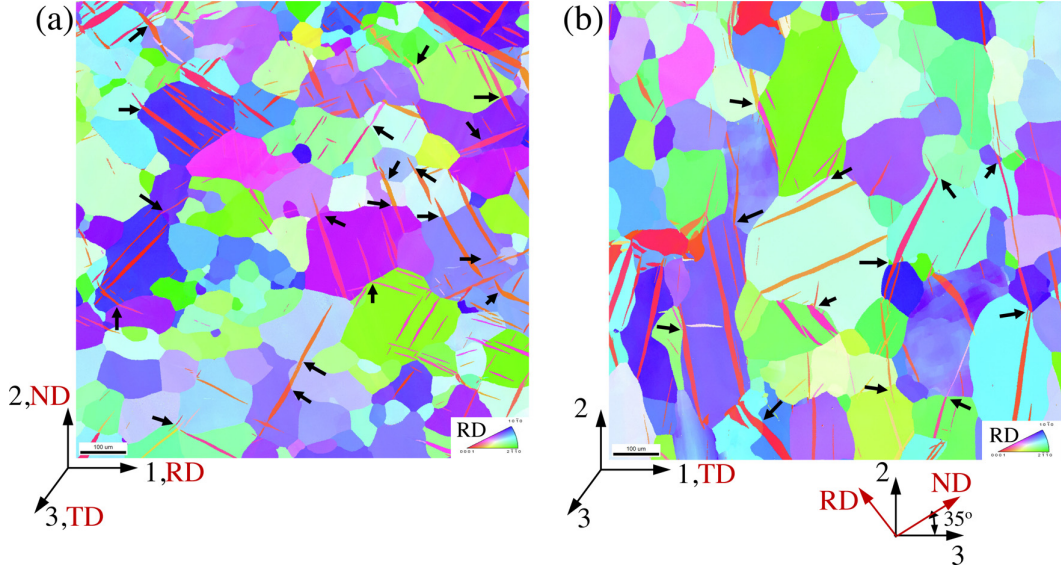


Fig. 5. A sample EBSD image of (a) a section containing RD and ND (section-1), and (b) a section with a normal at $\sim 35^\circ$ to the ND, and containing TD (section-2). Several twin transmissions on both sections can be seen, and a few are marked by black arrows.

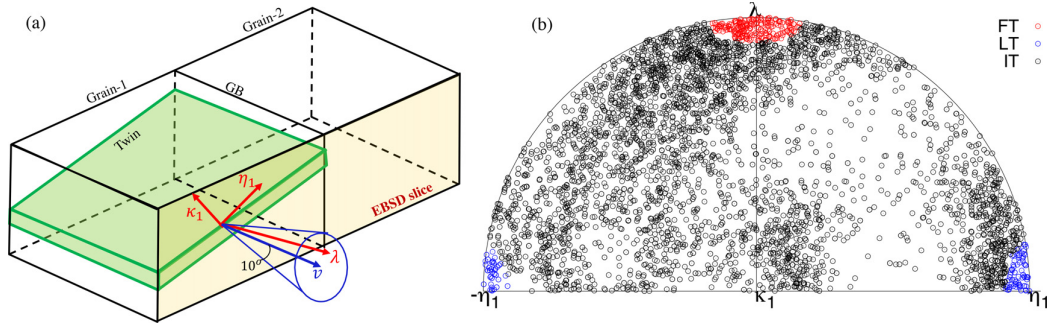


Fig. 6. Twin-GB interactions are classified as forward (FT), lateral (LT) and intermediate (IT) based on the EBSD slice viewing direction. For FT, $\widehat{v\lambda} < \phi$, whereas for LT, $\widehat{v\eta_1} < \phi$. Otherwise, twins are termed as IT. Here ϕ is the threshold angle, and it is set to be 10° . (a) Schematic representation of a forward twin-GB interaction. (b) Distribution of twin viewing direction (v) in the η_1 - λ - κ_1 space for all the twins. Based on this classification, out of 7213 twins, a total of 485, 277 and 6451 twins are identified as FT, LT, and IT, respectively.

λ -direction is close to the EBSD image viewing direction, v . Similarly, a twin will be deemed a LT if its η_1 direction is close to the viewing direction, v . Accordingly, for FT, $\widehat{v\lambda} < \phi$, whereas for LT, $\widehat{v\eta_1} < \phi$. Here ϕ is the threshold angle. Fig. 6(a) shows a schematic representation of twin-GB interactions along with the EBSD slice viewing direction. In this schematic the twin is interacting with the GB along its shear direction and thus it is referred to as FT. If a twin does not fall into one of these two cases, it is referred to as an intermediate direction twin (IT). In this work, thousands of twins are analyzed, and thus, it is anticipated that this approach provides reliable statistical information for TT propensity in the forward and lateral directions. Note, however, that a twin makes contact with GBs in all possible directions contained in the twinning plane. In this work, the threshold angle is set to be $\phi=10^\circ$. Accordingly, out of 7213 twins, 485 (6.7%), 277 (3.8%) and 6451 (89.4%) twins are identified as FT, LT and IT, respectively, and listed in Table 2. Fig. 6(b) shows these classified twins in the η_1 - λ - κ_1 space. As expected, based on the number fraction of FT or LT configurations, this analysis reveals that most of the twin-GB interactions are not purely forward or lateral. Also, note that the high number of points near the λ -direction is a natural consequence of the selected slicing geometries. That is, for the section-1, the viewing directions tend to cluster around λ ; and for the section-2, the viewing directions tend to cluster around η_1 and κ_1 .

Table 2

Statistical information of twins and their transmissions based on the viewing direction. Twin are classified as forward (FT), lateral (LT), and intermediate (IT) twins with a threshold angle of $\phi = 10^\circ$. ATPs are categorized as forward twin transmission (FTT), lateral twin transmission (LTT) and intermediate twin transmission (ITT).

Features		Number of data points
Total number of grains		3437
Number of twinned grains		1697
Total number of twins		7213
Number	FT	485 (6.7%)
of	LT	277 (3.8%)
	IT	6451 (89.44%)
Total number of ATPs		1708
Number	FTT	121.5 (7.1%)
of	LTT	90.5 (5.3%)
	ITT	1496 (87.6%)

From these three twin-GB interactions (FT, LT, and IT), nine different TT configurations can be formed, such as FT to FT, FT to LT, FT to IT, LT to FT, LT to LT, LT to IT, IT to FT, IT to LT and IT to IT. From the post-mortem EBSD images, it is not possible to identify the TT sequence. For

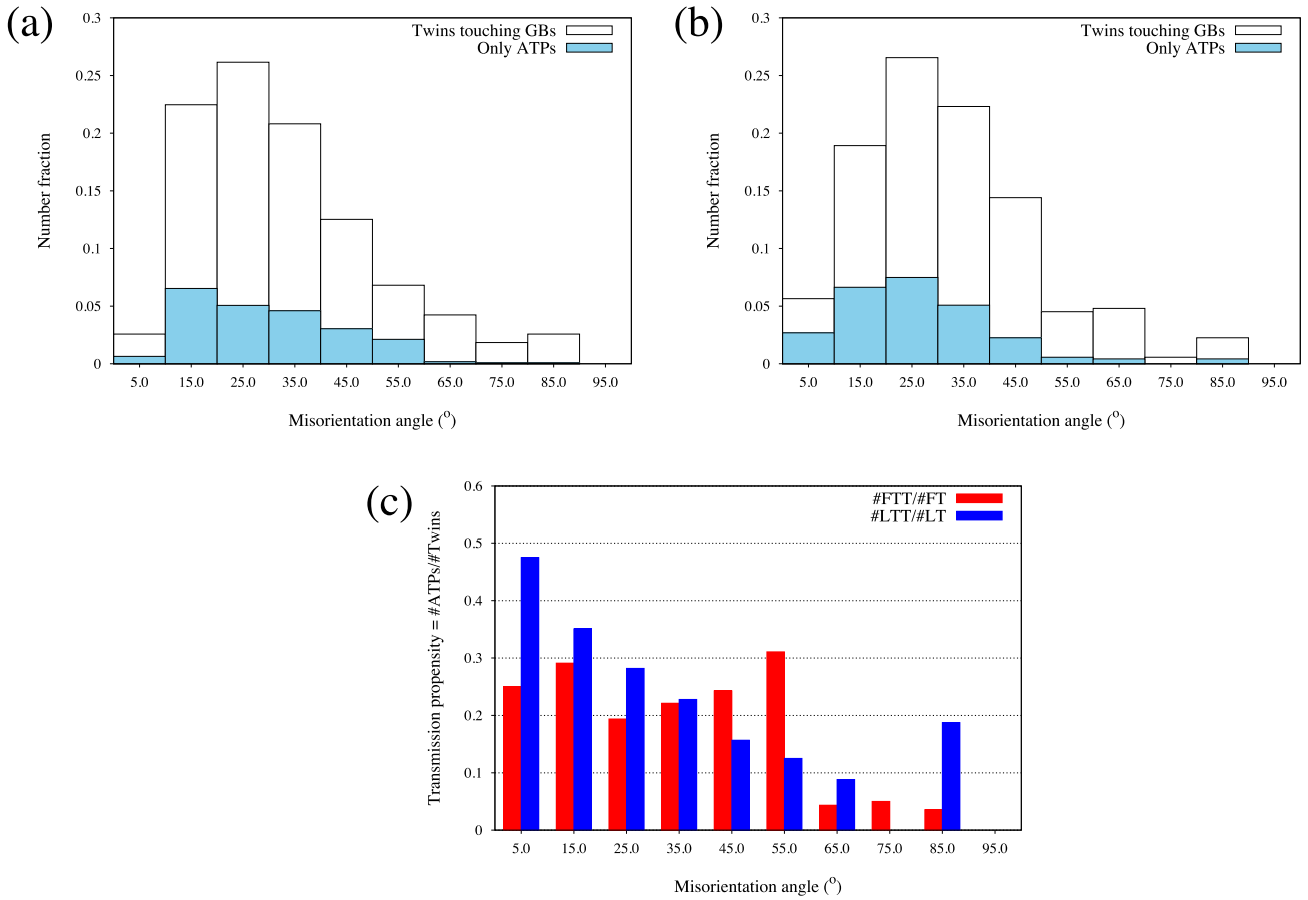


Fig. 7. Statistical distribution of twin-contacted GBs, and GBs with ATPs in the (a) forward and (b) lateral direction. White bars: GBs with either terminated or transmitted twins; blue bars: GBs with transmitted twins. (c) Twin transmission propensity (fraction of GBs with ATPs/ fraction of twin contacted GBs with twins) as a function of GB misorientation angle for both forward and lateral directions. The total number of FTTs and LTTs are 121.5 and 90.5, respectively. Similarly, the total number of FTs and LTs are 485 and 277, respectively.

example, an FT-LT configuration may be formed either by transmitting FT to LT or LT to FT. Thus, this ATP is assigned to both, forward and lateral twin transmission configurations, and will be counted as 0.5TT for both forward and lateral directions. Following this approach, ATPs are classified into three categories: forward twin transmission (FTT), lateral twin transmission (LTT) and intermediate twin transmission (ITT). The number of ATPs of different types is quantified and listed in Table 2. The possibility of FTT and LTT configurations is much less likely compared to ITT. For example, out of 1708 ATPs, only 121.5 (7.1%) and 90.5 (5.3%) ATPs are of FTT and LTT types. The remaining 87.6% of TT events occurs in directions not close to the forward or lateral directions.

Next, the effect of neighboring grains' misorientation angle on the forward and lateral transmission is analyzed. Fig. 7 shows the observed statistical correlation between misorientation angle across the GB and the likelihood of TT. Fig. 7(a) and (b) correspond to the statistical distribution for forward and lateral directions, respectively. The white and blue bars represent the number fraction of GBs with either terminated twins or ATPs, and the number fraction of GBs with ATPs, respectively. Fig. 7(c) shows the twinning propensity, which is defined as the fraction between the number of GBs with ATPs and the number of GBs with either terminated twins or ATPs. Fig. 7(c) shows the twinning propensity for both the forward and lateral directions. The number of ATPs beyond 45° is small, particularly for the lateral direction. Thus, we only consider the statistical correlations up to 45° Fig. 7(c) suggests that the propensity for TT decreases with increasing misorientation angle at the

GBs for the lateral directions, which supports the model predictions presented in Fig. 4. Such a clear correlation is not observed for the forward direction. Further, the twinning propensity is higher for the lateral side compared to the forward side, which also supports the model findings on the twin transmission bias.

The effect of misorientation axis between the grains on twin transmission is analyzed here. In Fig. 8, using stereographic projections, the GB misorientation axis is plotted in the local twin frame, η_1 - λ - κ_1 . This convention shows how the misorientation axis between the neighboring grains is oriented relative to the twin frame. For instance, a data point closer to the κ_1 coordinate represents the neighboring grains are misoriented by a rotation around the twin's κ_1 plane normal. This representation is exactly the same as the one used in Fig. 4. In Fig. 8, the left and right columns correspond to the forward and lateral TT, respectively. Misorientation axes are grouped in 10° GB misorientation angle intervals. The number of available data points for misorientation angles greater than 50° is small and so all the data points are plotted together. In Fig. 8, termination events are shown with empty circles, while transmission events are shown with filled circles. Note that a transmission event will appear twice in these maps: once for the initial and once for the transmitted twin. Fig. 8 suggests that those twins do not seem to require special/ideal misorientation axes for transmission to occur. Furthermore, Fig. 8 reveals that the possibility of having GBs misorientation axes aligned with the twin axes η_1 - λ - κ_1 , which represent pure tilt or pure twist grain misorientation conditions, is practically null. Thus,

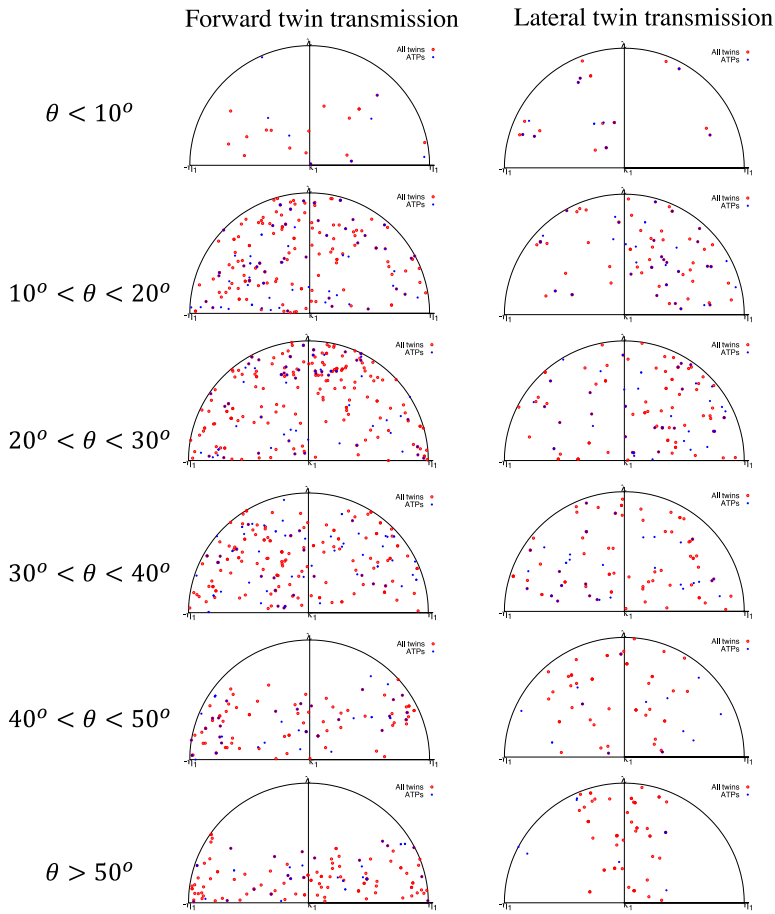


Fig. 8. Distribution of GB misorientation axis in the η_1 - λ - κ_1 space for misorientation angles, θ , ranges of: $[0^\circ, 10^\circ]$, $[10^\circ, 20^\circ]$, $[20^\circ, 30^\circ]$, $[30^\circ, 40^\circ]$, $[40^\circ, 50^\circ]$, and $>50^\circ$. The left and right columns correspond to forward and lateral twin-GB interactions, respectively. Empty circles: GBs with either terminated or transmitted twins; Filled circles (they superpose to the empty circles): GBs with twin transmission.

the conclusions derived from numerical simulations of such special and simpler configurations may not be representative of the actual deformed microstructure. However, the model calculations presented in this work with special GBs and simpler configurations help to understand and quantify the intrinsic bias in twin transmission between the bounding cases, i.e., forward and lateral directions.

5. Summary

In this work, a combined phase-field modeling and EBSD-based statistical analysis is performed to investigate twin transmission in Mg. The phase-field model reveals that twin transmission along the lateral direction is more favorable than along the forward direction, particularly as the misorientation angle increases. TT propensity decreases with increasing GB misorientation angle for both the forward and lateral directions. At the onset of transmission, the transmitted twin propagation/growth follows its crystallography in the case of lateral transmission, whereas, for the forward transmission case, the transmitted twin morphology nearly follows the initial twin-GB contact region, not its crystallography. Twin transmission seems harder across GBs with misorientation axes closer to the twin λ -direction compared to the other directions (κ_1 and η_1). EBSD based statistical analysis finds that the twin transmission along the forward and lateral directions statistically occurs less compared to directions between them. The probability of having pure tilt or twist GBs in the actual material is almost null. Thus, the commonly considered simple symmetric GB configurations for the numerical simulations may not be representative. Further, EBSD results do not reveal any preference on the misorientation axis between the grains for twin transmission to occur. Similar to the phase-field model,

the EBSD-based analysis shows that the twin transmissibility decreases with GB misorientation angle and it is relatively harder for the forward direction compared to the lateral direction. In practice though these configurations represent less than 10 percent of observed transmission events.

Declaration of Competing Interest

The authors declare that they have no known competing financial interests or personal relationships that could have appeared to influence the work reported in this paper.

Acknowledgments

This work is fully funded by the U.S. Dept. of Energy, Office of Basic Energy Sciences Project FWP 06SCPE401. This research used resources provided by the Los Alamos National Laboratory Institutional Computing Program, which is supported by the U.S. Department of Energy National Nuclear Security Administration under Contract No. 89233218CNA000001

Supplementary materials

Supplementary material associated with this article can be found, in the online version, at doi:[10.1016/j.mtla.2022.101437](https://doi.org/10.1016/j.mtla.2022.101437).

References

- [1] I.J. Beyerlein, R.J. McCabe, C.N. Tome, Effect of microstructure on the nucleation of deformation twins in polycrystalline high-purity magnesium: a multi-scale modeling study, *J. Mech. Phys. Solids* 59 (5) (2011) 988–1003.

- [2] I.J. Beyerlein, C.N. Tome, A probabilistic twin nucleation model for HCP polycrystalline metals, *Proc. R. Soc. Math. Phys. Eng. Sci.* 466 (2121) (2010) 2517–2544.
- [3] J. Wang, I.J. Beyerlein, C.N. Tome, An atomic and probabilistic perspective on twin nucleation in Mg, *Scr. Mater.* 63 (7) (2010) 741–746.
- [4] J. Wang, S.K. Yadav, J.P. Hirth, C.N. Tome, I.J. Beyerlein, Pure-shuffle nucleation of deformation twins in hexagonal-close-packed metals, *Mater. Res. Lett.* 1 (3) (2013) 126–132.
- [5] C.D. Barrett, H. El Kadiri, The roles of grain boundary dislocations and disclinations in the nucleation of $\{10\bar{1}1\}$ twinning, *Acta Mater.* 63 (2014) 1–15.
- [6] Y. Liu, N. Li, S. Shao, M. Gong, J. Wang, R.J. McCabe, Y. Jiang, C.N. Tomé, Characterizing the boundary lateral to the shear direction of deformation twins in magnesium, *Nat. Commun.* 7 (2016) 11577.
- [7] Y. Liu, P.Z. Tang, M.Y. Gong, R.J. McCabe, J. Wang, C.N. Tomé, Three dimensional character of $\{10\bar{1}2\}$ deformation twin in Mg, *Nat. Commun.* 10 (2019) 3308.
- [8] M.A. Kumar, A.K. Kanjarla, S.R. Niezgodza, R.A. Lebensohn, C.N. Tome, Numerical study of the stress state of a deformation twin in magnesium, *Acta Mater.* 84 (2015) 349–358.
- [9] R. McCabe, M.A. Kumar, W. Liu, C. Tomé, L. Capolungo, Revealing the effect of local stresses on twin growth mechanisms in titanium using synchrotron X-ray diffraction, *Acta Mater.* 221 (2021) 117359.
- [10] M.A. Kumar, I.J. Beyerlein, C.N. Tome, Effect of local stress fields on twin characteristics in HCP metals, *Acta Mater.* 116 (2016) 143–154.
- [11] S.M. Yin, F. Yang, X.M. Yang, S.D. Wu, S.X. Li, G.Y. Li, The role of twinning-de-twinning on fatigue fracture morphology of Mg-3%Al-1%Zn alloy, *Mater. Sci. Eng. Struct. Mater. Prop. Microstruct. Process.* 494 (1–2) (2008) 397–400.
- [12] B.A. Simkin, B.C. Ng, M.A. Crimp, T.R. Bieler, Crack opening due to deformation twin shear at grain boundaries in near-gamma TiAl, *Intermetallics* 15 (1) (2007) 55–60.
- [13] F. Yang, S.M. Yin, S.X. Li, Z.F. Zhang, Crack initiation mechanism of extruded AZ31 magnesium alloy in the very high cycle fatigue regime, *Mater. Sci. Eng. Struct. Mater. Prop. Microstruct. Process.* 491 (1–2) (2008) 131–136.
- [14] D.E. Spearot, V. Taupin, K. Dang, L. Capolungo, Structure and kinetics of three-dimensional defects on the $\{10\bar{1}2\}$ twin boundary in magnesium: atomistic and phase-field simulations, *Mech. Mater.* 143 (2020) 103314.
- [15] C.N. Tomé, M.A. Kumar, J. Graham, K. Dang, Y. Liu, P. Tang, S. Wang, R.J. McCabe, L. Capolungo, Twin transmission across grain boundaries in Mg, in: *Magnesium Technology 2020*, Springer, 2020, pp. 3–5.
- [16] K. Dang, J. Graham, R. McCabe, V. Taupin, C. Tomé, L. Capolungo, Atomistic and phase field simulations of three dimensional interactions of $\{10\bar{1}2\}$ twins with grain boundaries in Mg: twin transmission and dislocation emission, *Materialia* 20 (2021) 101247.
- [17] M. Gong, J. Graham, V. Taupin, L. Capolungo, The effects of stress, temperature and facet structure on growth of $\{10\bar{1}2\}$ twins in Mg: a molecular dynamics and phase field study, *Acta Mater.* 208 (2021) 116603.
- [18] A. Fernández, A. Jérusalem, I. Gutiérrez-Urrutia, M. Pérez-Prado, Three-dimensional investigation of grain boundary–twin interactions in a Mg AZ31 alloy by electron backscatter diffraction and continuum modeling, *Acta Mater.* 61 (20) (2013) 7679–7692.
- [19] F. Ram, J.T. Lloyd, G.S. Rohrer, Habit planes of twins in a deformed Mg alloy determined from three-dimensional microstructure analysis, *Mater. Charact.* 159 (2020) 110014.
- [20] S. Wang, M. Gong, R.J. McCabe, L. Capolungo, J. Wang, C.N. Tomé, Characteristic boundaries associated with three-dimensional twins in hexagonal metals, *Sci. Adv.* 6 (28) (2020) eaaz2600.
- [21] S. Wang, K. Dang, R.J. McCabe, L. Capolungo, C.N. Tomé, Three-dimensional atomic scale characterization of $\{11\bar{2}2\}$ twin boundaries in titanium, *Acta Mater.* 208 (2021) 116707.
- [22] M.R. Barnett, M.D. Nave, A. Ghaderi, Yield point elongation due to twinning in a magnesium alloy, *Acta Mater.* 60 (4) (2012) 1433–1443.
- [23] I.J. Beyerlein, L. Capolungo, P.E. Marshall, R.J. McCabe, C.N. Tome, Statistical analyses of deformation twinning in magnesium (vol 90, pg 2161, 2010), *Philos. Mag.* 90 (30) (2010) 4073–4074.
- [24] C.F. Guo, R.L. Xin, C.H. Ding, B. Song, Q. Liu, Understanding of variant selection and twin patterns in compressed Mg alloy sheets via combined analysis of Schmid factor and strain compatibility factor, *Mater. Sci. Eng. Struct. Mater. Prop. Microstruct. Process.* 609 (2014) 92–101.
- [25] A. Khosravani, D.T. Fullwood, B.L. Adams, T.M. Rampton, M.P. Miles, R.K. Mishra, Nucleation and propagation of $\{10\bar{1}1\}$ twins in AZ31 magnesium alloy, *Acta Mater.* 100 (2015) 202–214.
- [26] M.A. Kumar, I.J. Beyerlein, R.A. Lebensohn, C.N. Tome, Role of alloying elements on twin growth and twin transmission in magnesium alloys, *Mater. Sci. Eng. Struct. Mater. Prop. Microstruct. Process.* 706 (2017) 295–303.
- [27] M.A. Kumar, I.J. Beyerlein, R.J. McCabe, C.N. Tome, Grain neighbour effects on twin transmission in hexagonal close-packed materials, *Nat. Commun.* 7 (2016) 13826 Article.
- [28] Z.Z. Shi, Y.D. Zhang, F. Wagner, P.A. Juan, S. Berbenni, L. Capolungo, J.S. Lecomte, T. Richeton, On the selection of extension twin variants with low Schmid factors in a deformed Mg alloy, *Acta Mater.* 83 (2015) 17–28.
- [29] R.L. Xin, Y.C. Liang, C.H. Ding, C.F. Guo, B.S. Wang, Q. Liu, Geometrical compatibility factor analysis of paired extension twins in extruded Mg-3Al-1Zn alloys, *Mater. Des.* 86 (2015) 656–663.
- [30] M.A. Kumar, L. Capolungo, R.J. McCabe, C.N. Tomé, Characterizing the role of adjoining twins at grain boundaries in hexagonal close packed materials, *Sci. Rep.* 9 (1) (2019) 3846.
- [31] T. Bieler, L. Wang, A. Beaudoin, P. Kenesei, U. Lienert, *In situ* characterization of twin nucleation in pure Ti using 3D-XRD, *Metall. Mater. Trans. Phys. Metall. Mater. Sci.* 45A (1) (2014) 109–122.
- [32] L. Wang, P. Eisenlohr, Y. Yang, T.R. Bieler, M.A. Crimp, Nucleation of paired twins at grain boundaries in titanium, *Scr. Mater.* 63 (8) (2010) 827–830.
- [33] J. Kacher, A.M. Minor, Twin boundary interactions with grain boundaries investigated in pure rhenium, *Acta Mater.* 81 (2014) 1–8.
- [34] C. Pradalier, P.A. Juan, R.J. McCabe, L. Capolungo, A graph theory-based automated twin recognition technique for electron backscatter diffraction analysis, *Integr. Mater. Manuf. Innov.* 7 (1) (2018) 12–27.
- [35] S.M. Allen, J.W. Cahn, A microscopic theory for antiphase boundary motion and its application to antiphase domain coarsening, *Acta Metall.* 27 (6) (1979) 1085–1095.
- [36] I. Basu, H. Fidler, V. Ocelik, J.T.M. de Hosson, Local stress states and microstructural damage response associated with deformation twins in hexagonal close packed metals, *Crystals* 8 (1) (2018) 1–15 Article 1.
- [37] Y. Guo, H. Abdolvand, T.B. Britton, A.J. Wilkinson, Growth of $\{11\bar{2}2\}$ twins in titanium: a combined experimental and modelling investigation of the local state of deformation, *Acta Mater.* 126 (2017) 221–235.
- [38] M.A. Kumar, B. Clausen, L. Capolungo, R.J. McCabe, W. Liu, J.Z. Tischler, C.N. Tome, Deformation twinning and grain partitioning in a hexagonal close-packed magnesium alloy, *Nat. Commun.* 9 (2018) 4761.
- [39] M.A. Kumar, I.J. Beyerlein, R.A. Lebensohn, C.N. Tome, Modeling the effect of neighboring grains on twin growth in HCP polycrystals, *Modell. Simul. Mater. Sci. Eng.* 25 (6) (2017) 1–25 Article 064007.